ANL/ENG-80-02

ARGONNE NATIONAL LABORATORY
9700 South Cass Avenue
Argonne, Illinois 60439

A STUDY OF PIPING CONFIGURATIONS*

by

Y. Pan, A. Rafer and H. Ahmed

Design Engineering Analysis

Engineering Division

January 1980

*This work was performed under the auspices of U. S. Department of Energy.

DISCLAIMER

ANL/ENG-80-02

ARGONNE NATIONAL LABORATORY
9700 South Cass Avenue
Argonne, Illinois 60439

A STUDY OF PIPING CONFIGURATIONS*

by

Y. Pan, A. Rafer and H. Ahmed

Design Engineering Analysis

Engineering Division

January 1980

*This work was performed under the auspices of U. S. Department of Energy.

ACKNOWLEDGEMENTS

The authors wish to express their gratitude to Mr. A. Amorosi who made this study possible under a larger conceptual design study of loop type LMFBRs at ANL.

ABSTRACT

A study of piping and elbow flexibility is performed using an analytical approach and piping analysis computer programs ADLPIPE and MARC. The study focuses on pipe loop configurations commonly used to accommodate thermal expansion in such applications as Liquid Metal Fast Breeder Reactors.

TABLE OF CONTENTS

LIST OF FIGURES

LIST OF FIGURES
(cont.)

A STUDY OF PIPING CONFIGURATIONS

I.0 Introduction

In the design of a piping system which is subject to high operating temperature, an expansion loop is commonly used to accommodate thermal expansion. The basic components of an expansion loop include the straight pipes and pipe bends (elbows). It is of interest in the design of a piping system to learn how different piping configurations behave under thermal loading. Therefore, this study is made to try to assess the relative merit of some selected configurations that might be used in the LMFBR piping design to accommodate thermal expansion. The configurations examined are the hairpin loop, the U-bend loop, the coil loop and the omega loop. The thermal expansion is treated as a constant anchor movement in the analysis. The thermal stresses are calculated by both the analytic method and the finite element computer method in accordance with ASME Pressure Vessel and Piping Code [1].

II.0 Analytic Method

Each piping configuration is analyzed by the conventional beam method [2]. The additional flexibility of the pipe bend due to the ovalization of the cross section is accommodated by including the flexibility factor in the moment-curvature relation. The force and moment acting on the pipe are obtained by using the Castigliano theorem. The stresses in each cross section are then calculated according to the simplified equations given in the ASME Pressure Vessel and Piping Code Section III Subsection NA [1]. These equations contain the stress intensification factor for the pipe bend. A typical example of the analysis is given in the following for a

hairpin loop fixed at both ends and subjected to a constant displacement in the Z-direction as shown in Figure II.1.a.

Due to symmetry, only half of the hairpin loop needs to be analyzed. The free body diagram of the loop is shown in Figure II.1.b. The elastic energy of a straight beam subjected to pure bending is given by [2]

$$E_s = \int \frac{M^2}{2EI}\, d\ell \tag{II.1}$$

where M is the applied moment, E is the Young's modulus, I is the moment of inertia of the cross section, and $d\ell$ is the incremental length of the pipe. For a pipe bend, the following equation must be used

$$E_b = \int k\, \frac{M^2}{2EI}\, d\ell \tag{II.2}$$

where k is the flexibility factor of the elbow. Based on Eqs. (II.1) and (II.2), the elastic energy of the pipe is

$$E = \int_o^{\ell} \frac{(FX - M)^2}{2EI}\, dx + \int_o^{\pi/2} k\, \frac{[F(\ell + R \sin\theta) - M]^2}{2EI}\, Rd\theta. \tag{II.3}$$

From Castigliano theory, the slope at the end of the pipe can be found by

$$\phi = \frac{\partial E}{\partial M} = 0 = \int_o^{\ell} \frac{M - FX}{EI}\, dx + \frac{kR}{EI} \int_o^{\pi/2} [M - F(\ell + R \sin\theta)]d\theta$$

$$= \frac{M}{EI}\left[\ell + \frac{\pi}{2}kR\right] - \frac{F}{EI}\left[\frac{\ell^2}{2} + kR\left(\frac{\pi}{2}\ell + R\right)\right]. \tag{II.4}$$

Eq. (II.4) has the solution

$M = F\xi$,

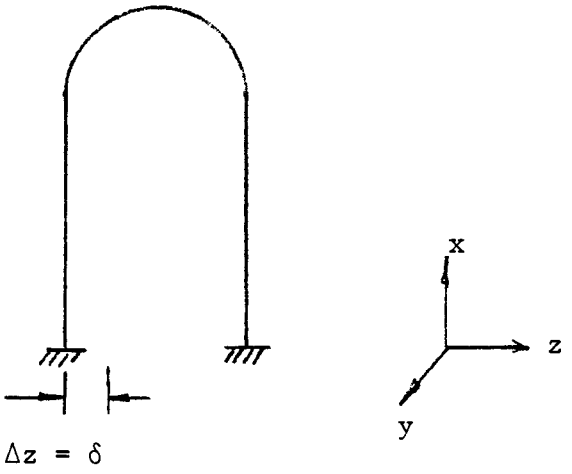

(a)

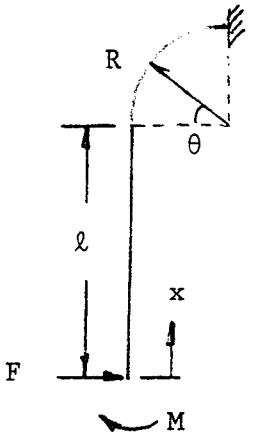

(b)

Figure II.1. A Hairpin Loop Subjected to A Constant Anchor Movement in the Z-Direction.

where (II.5)

$$\xi = \frac{\frac{\ell^2}{2} + kR(\frac{\pi}{2}\ell + R)}{\ell + \frac{\pi}{2} kR} .$$

The deflection at the end of the pipe is given by

$$\delta = \frac{\partial E}{\partial F} = \int_o^{\ell} \frac{FX^2 - Mx}{EI} dx + \int_o^{\pi/2} \frac{kR}{EI} [F(\ell^2 + 2R\ell \text{ Sin } \theta + R^2 \text{ Sin}^2\theta) -$$

$$M(\ell + R \text{ Sin } \theta)]d\theta$$

$$= \frac{F}{EI} \left\{ \frac{\ell^3}{3} + kR(\frac{\pi}{2}\ell^2 + 2R\ell + \frac{\pi}{4}R^2) - \xi[\frac{\ell^2}{2} + kR(\frac{\pi}{2}\ell + R)] \right\} . \quad (II.6)$$

Hence,

$$F = \frac{\delta EI}{\Delta} \quad (II.7)$$

where

$$\Delta = \frac{\ell^3}{3} + kR(\frac{\pi}{2}\ell^2 + 2R\ell + \frac{\pi}{4}R^2) - \xi[\frac{\ell^2}{2} + kR(\frac{\pi}{2}\ell + R)]$$

Once the reacting force and moment are found, the moment at any cross section is given as

$$M_x = M - FX = F(\xi - X) \quad (II.8)$$

where ξ is given in Eq. (II.5) and $x = \ell + R \sin\theta$ if $x > \ell$. Therefore, the stress in the U-bend is

$$\sigma = \frac{Mx}{Z} = \frac{F}{Z}(\xi - X) \qquad x \leq \ell$$

$$\sigma = B\frac{Mx}{Z} = \frac{B}{Z}[F\xi - F(\ell + R \sin\theta)] \qquad x \geq \ell \tag{II.9}$$

where Z is the section modulus and B is the stress intensification factor for the elbow.

The flexibility factor and the stress intensification factor can be found in the ASME Pressure Vessel and Piping Code [1]. For a Class 1 nuclear component,

$$k = \frac{1.65}{h} \qquad \text{for in-plane and out-of-plane bending}$$

$$= 1 \qquad \text{for twisting}$$

$$B = 0.75\frac{1.95}{(h)^{2/3}} \tag{II.10}$$

where $h = \frac{tR}{r^2}$, t is the thickness of the pipe, r is the mean radius of the pipe and R is the radius of the pipe bend. When all three components of the bending moment exist, the resultant moment as defined in the Code is used to calculate the stress.

$$M = (M_x^2 + M_y^2 + M_z^2)^{1/2} \tag{II.11}$$

The flexibility factors and the stress intensification factors are calculated for different pipe sizes and elbow radii and are plotted in Figures (II.2) to (II.3). It is noted that both the flexibility factor and the stress intensification factor decrease with increasing pipe thickness and bend radius or decreasing pipe diameter.

The equations for other piping configurations can be obtained in a similar manner and the results are summarized in the following. In these equations F and M denotes the anchor reactive force and reactive moment, respectively. The subscripts x, y, and z denote components in the x, y, and z directions, respectively. If a component is not given, it is defaulted to zero. Once the anchor forces and moments are known, the bending moment in any cross section can be found and the maximum stress in that cross section can be calculated by

$$\sigma = \frac{M}{Z} \qquad \text{(straight pipe)}$$

$$\sigma = B\frac{M}{Z} \qquad \text{(elbow)} \qquad \text{(II.12)}$$

where B is given in Eq. (II.10)

A) Hairpin shapped piping (Fig. II.1a) fixed at both ends and subjected to an anchor displacement δ in the x-direction:

$$F_x = \frac{\delta EI}{\Delta}$$

$$M_y = -F_x R$$

$$\Delta = R^2 \ell + \frac{\pi}{4} kR^3 \qquad \text{(II.13)}$$

B) Hairpin shapped piping (Fig. II.1a) fixed at both ends and subjected to an anchor displacement δ in the y direction:

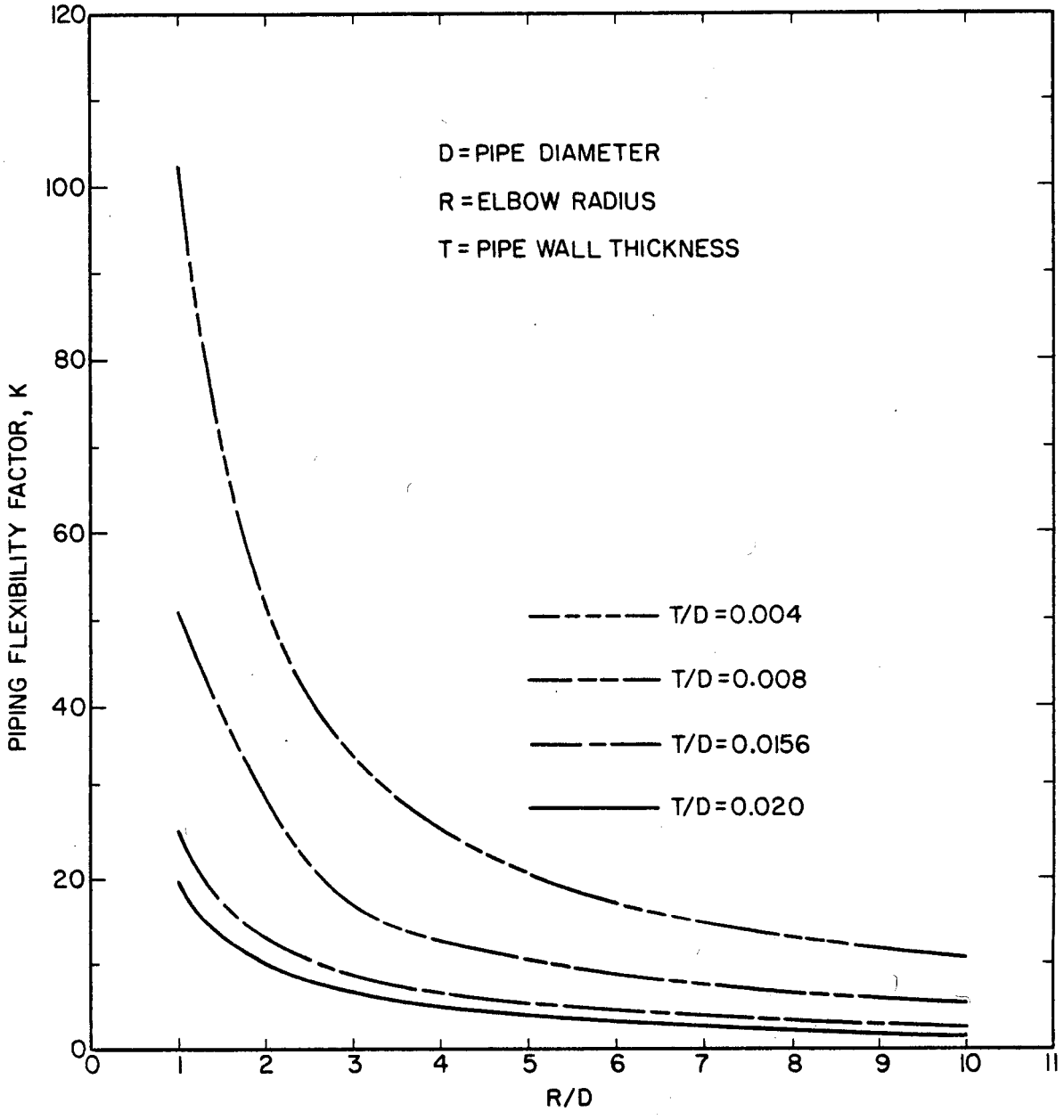

Figure II.2 Piping Flexibility Factor

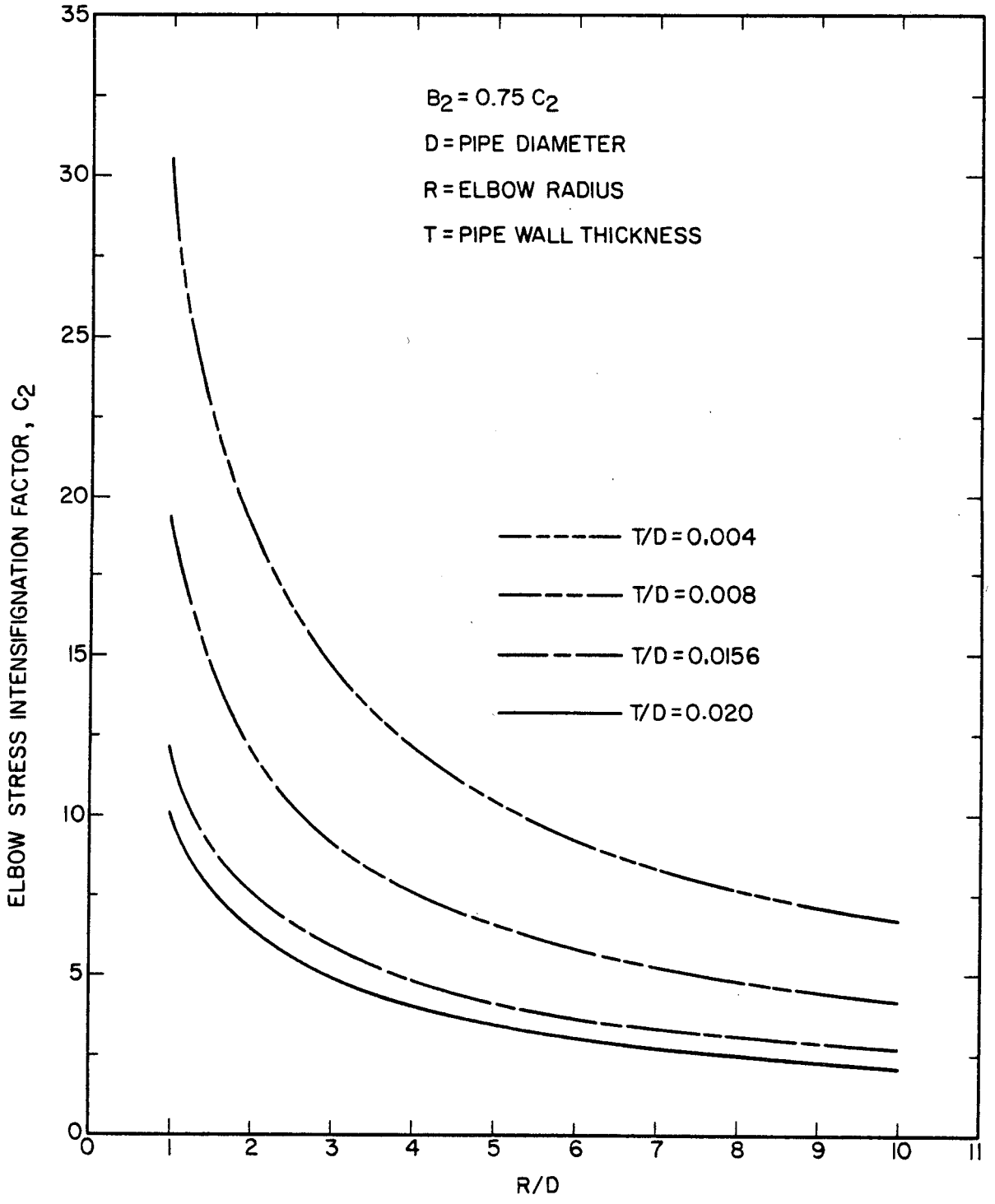

Figure II.3 Elbow Stress Intensification Factor

$$F_y = \frac{\delta EI}{\Delta}$$

$$M_x = - F_y R$$

$$M_z = - F\xi$$

$$\xi = \frac{\frac{\ell^2}{2} + \frac{\pi}{4} kR\ell + \frac{1}{3} kR^2}{\ell + \frac{\pi}{4} kR}$$

$$\Delta = \frac{\ell^3}{3} + kR \left(\frac{\pi}{4} \ell^2 + \frac{2}{3} R\ell + \frac{1}{4} R^2\right) - \xi\left(\frac{\ell^2}{2} + \frac{\pi}{4} kR\ell + \frac{1}{3} kR^2\right) \qquad \text{(II.14)}$$

C) Two hump piping (Fig. II.4) hinged at both ends and subjected to an anchor displacement δ in the z-direction:

$$F_z = \frac{\delta EI}{\Delta}$$

$$F_x = \frac{\ell_1 - \ell_2}{2R} F_z$$

$$\Delta = \frac{2}{3} \ell_1^3 + \frac{2}{3} (\ell_1 - \ell_2)^3 - (\ell_1 - \ell_2)\ell_1^2 + \ell_2(\ell_1 - \ell_2)^2$$

$$+ kR\left[\frac{\pi}{2}R^2 + \pi\ell_1\ell_2 + 2R(\ell_1 + \ell_2) + \frac{3}{8}\pi(\ell_1 - \ell_2)^2\right] \qquad \text{(II.15)}$$

D) Two hump piping (Fig. II.4) hinged at both ends and subjected to an anchor displacement δ in the x-direction:

$$F_x = \frac{\delta EI}{\Delta} \left(\frac{\ell_1 - \ell_2}{2R}\right)^2$$

$$F_z = \frac{2R}{\ell_1 - \ell_2} F_x \qquad \text{(II.16)}$$

where Δ is given in Eq. (II.15).

E) Three hump piping (Fig. II.5) hinged at both ends and subjected to anchor displacement δ in the z-direction:

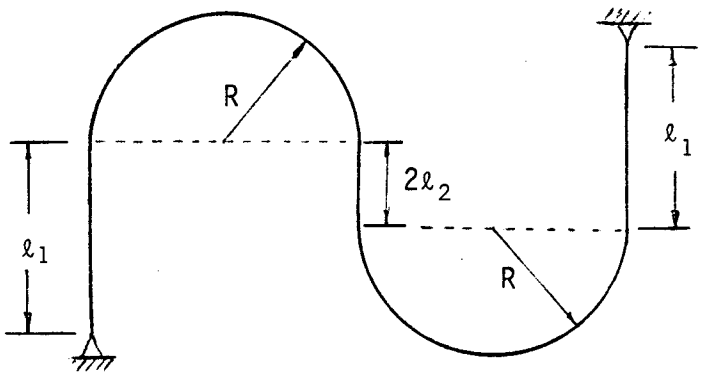

FIG. II.4 Piping Configuration Containing Two 180° Elbows

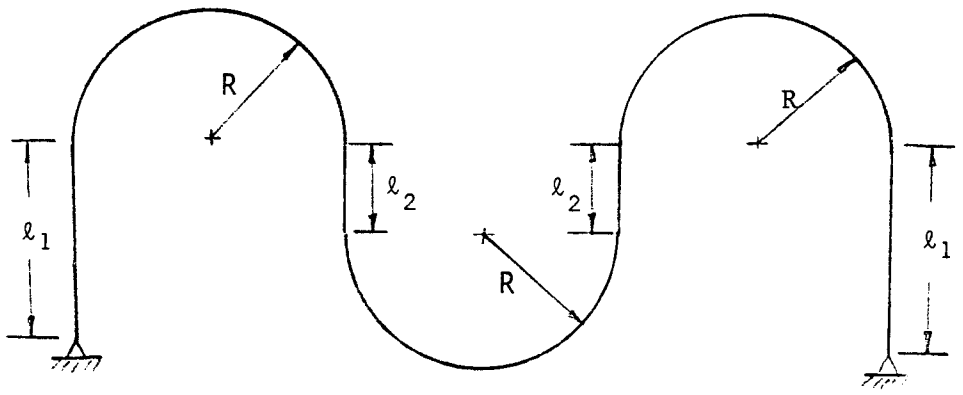

FIG. II.5 Piping Configuration Containing Three 180° Elbows

$$F_z = \frac{\delta EI}{\Delta}$$

$$\Delta = \frac{2}{3}\ell_1^3 - \frac{1}{3}(\ell_1 - \ell_2)^3 + k[\pi R\ell_1^2 + \frac{\pi R}{2}(\ell_1 - \ell_2)^2 + \frac{3}{4}\pi R^3 -$$

$$2R^2(\ell_1 - \ell_2) + 4R^2\ell_1] \qquad \text{(II.17)}$$

F) Four hump piping (Fig. II.6) hinged at both ends and subjected to an anchor displacement δ in the z-direction:

$$F_z = \frac{\delta EI}{\Delta}$$

$$F_x = \frac{\ell}{4R} F_z$$

$$\Delta = \frac{\ell^3}{3} + kR\ [\pi R^2 + \frac{11}{16}\pi\ell^2 + 2R\ell] \qquad \text{(II.18)}$$

G) Four hump piping (Fig. II.6) hinged at both ends and subjected to an anchor displacement δ in the x-direction:

$$F_x = \frac{\delta EI}{\Delta}$$

$$F_z = \frac{4R}{\ell} F_x$$

$$\Delta = (\frac{4R}{\ell})^2\ [\frac{\ell^3}{3} + kR(\pi R^2 + \frac{11}{16}\pi\ell^2 + 2R\ell)] \qquad \text{(II.19)}$$

H) Coil shaped piping (Fig. II.7) hinged at both ends and subjected to an anchor displacement δ in the z-direction:

$$F_z = \frac{\delta EI}{\Delta}$$

$$\Delta = \frac{3}{2}\pi kR^3 \qquad \text{(II.20)}$$

I) U-shaped piping (Fig. II.8) hinged at both ends and subjected to an anchor displacement δ in the z-direction:

$$F_z = \frac{\delta EI}{\Delta}$$

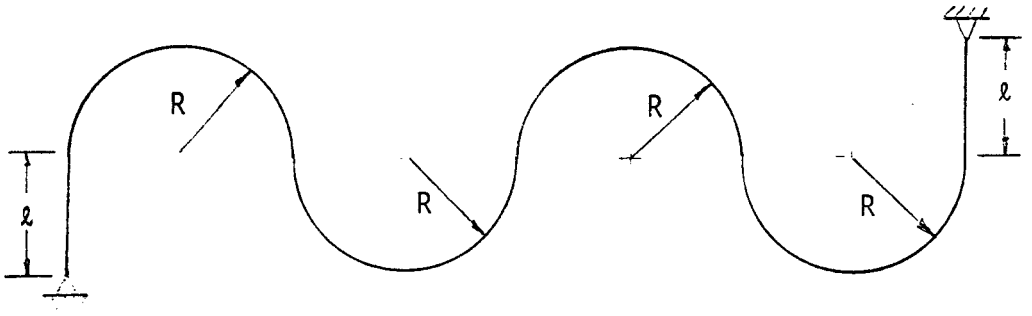

FIG. II.6 Piping Configuration Containing Four 180° Elbows

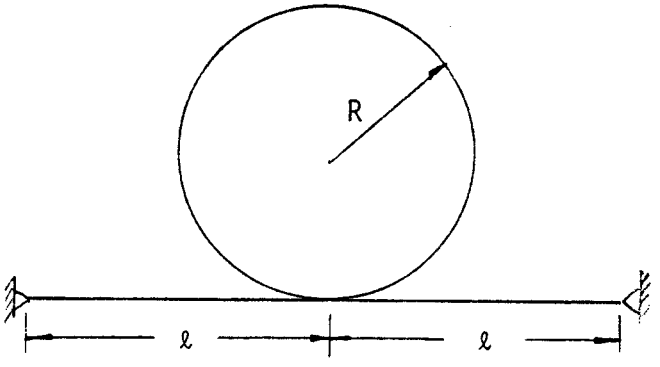

FIG. II.7 Coil Shaped Piping Configuration

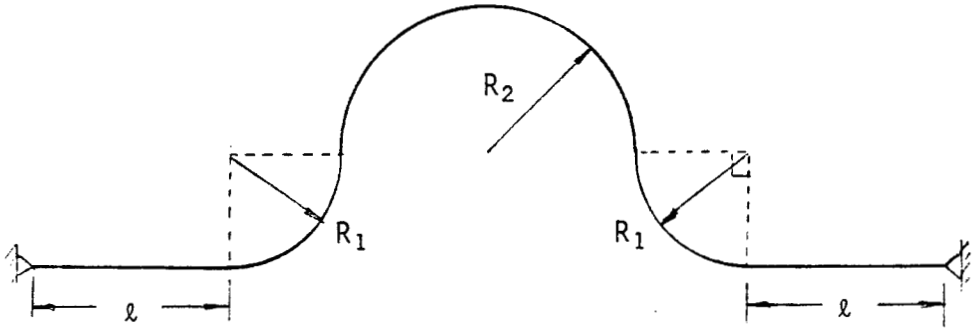

FIG. II.8 U Shaped Piping Configuration

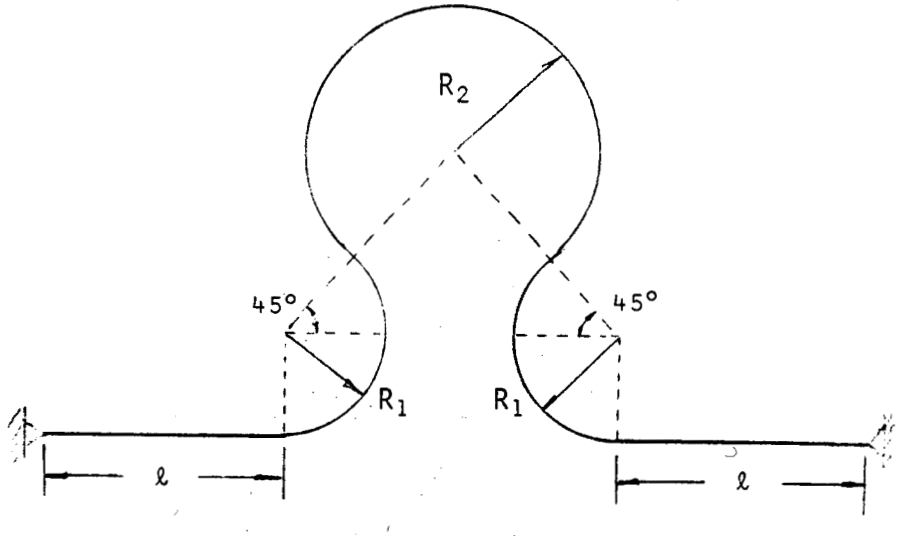

FIG. II.9 Omega Shaped Piping Configuration

$$\Delta = k_1[\frac{3}{4}\pi R_1^3 - 2R_1^3] + k_2[\frac{\pi}{2}R_1^2R_2 + 2R_1R_2^2 + \frac{1}{4}\pi R_2^3] \qquad \text{(II.21)}$$

J) Omega shaped piping (Fig. II.9) hinged at both ends and subjected to an anchor displacement δ in the z-direction:

$$F_z = \frac{\delta EI}{\Delta}$$

$$\Delta = k_1R_1^3(\frac{9\pi}{8} - \sqrt{2} - \frac{1}{4}) + k_2R_2(\frac{3}{4}\pi\ell_2^2 + \sqrt{2}R_2\ell_2 + \frac{3\pi}{8}R_2^2 - \frac{R_2^2}{4}) \qquad \text{(II.22)}$$

III.0 Finite Element Method

There are several finite element programs which can be used to analyze a piping system. The programs which are used in this study are the ADLPIPE and MARC computer programs.

III.1 ADLPIPE Computer Analysis

This program uses the conventional beam method to analyze a piping system according to the ASME Pressure Vessel and Piping Code. Two sets of studies were made. The first set of study examines various selected configurations with constant length of 100'. The pipe diameter is 48" and the pipe thickness is 0.75". These dimensions are selected because they are used in the LMFBR loop study [3]. The output of the computer calculation has been checked against the analytic results. The maximum deviation is found to be 5%. The result of the analysis is shown in Figures (III.1) to (III.10).

Figure III.1 (a) shows the stress distribution along a 100' constant length pipe for a 1" anchor displacement in the X-direction. The reactive anchor force is in the X-direction and the reactive moment is in the Y-direction. Hence the moment and the bending stress is constant along the straight pipe. The stress shows a jump at the junction of the straight

pipe and the elbow due to the stress intensification factor of the elbow as indicated in Eq. (II.9). In the elbow, the moment and the stress decreases to zero at the symmetry point.

In Figure III.1 (b) anchor forces and moments in all X, Y and Z directions are non-zero. The resultant moment is calculated according to Eq. (II.11). Hence the stress distribution is non-linear along the straight pipe. The stress again shows a jump at the junction of straight pipe and elbow due to the stress intensification.

In Figure III.1 (c) the stress distribution along the straight pipe is linear since the anchor force is in the Z-direction and the anchor moment is in the Y-direction. The resultant moment in the straight pipe section is always in the Y-direction. The stress curve at the elbow first falls then rises as the moment goes to zero and changes sign in the elbow.

Figure III.1 (d) shows the maximum stress for different bend radii. In general, the stress decreases as the bend radius increases. The only exception occurs when the anchor displacement is in the Z-direction where the maximum stress increases. This is because increasing the bend radius reduces the straight pipe length for a constant length pipe. A constant anchor displacement means more elbow deflection for a larger bend radius, hence the maximum stress increases.

Figure III.2 to Figure III.4 can be explained in the same manner as Figure III.1. The general trend is for the stress to go down as the number of elbows increases or the elbow radius increases. As indicated in Figure III.1 (c), the only exception is when the anchor displacement is in the Z-direction. In that case, the trend is for the stress to go up as the number of elbow or the elbow radius decreases due to the shortening of the straight pipe section.

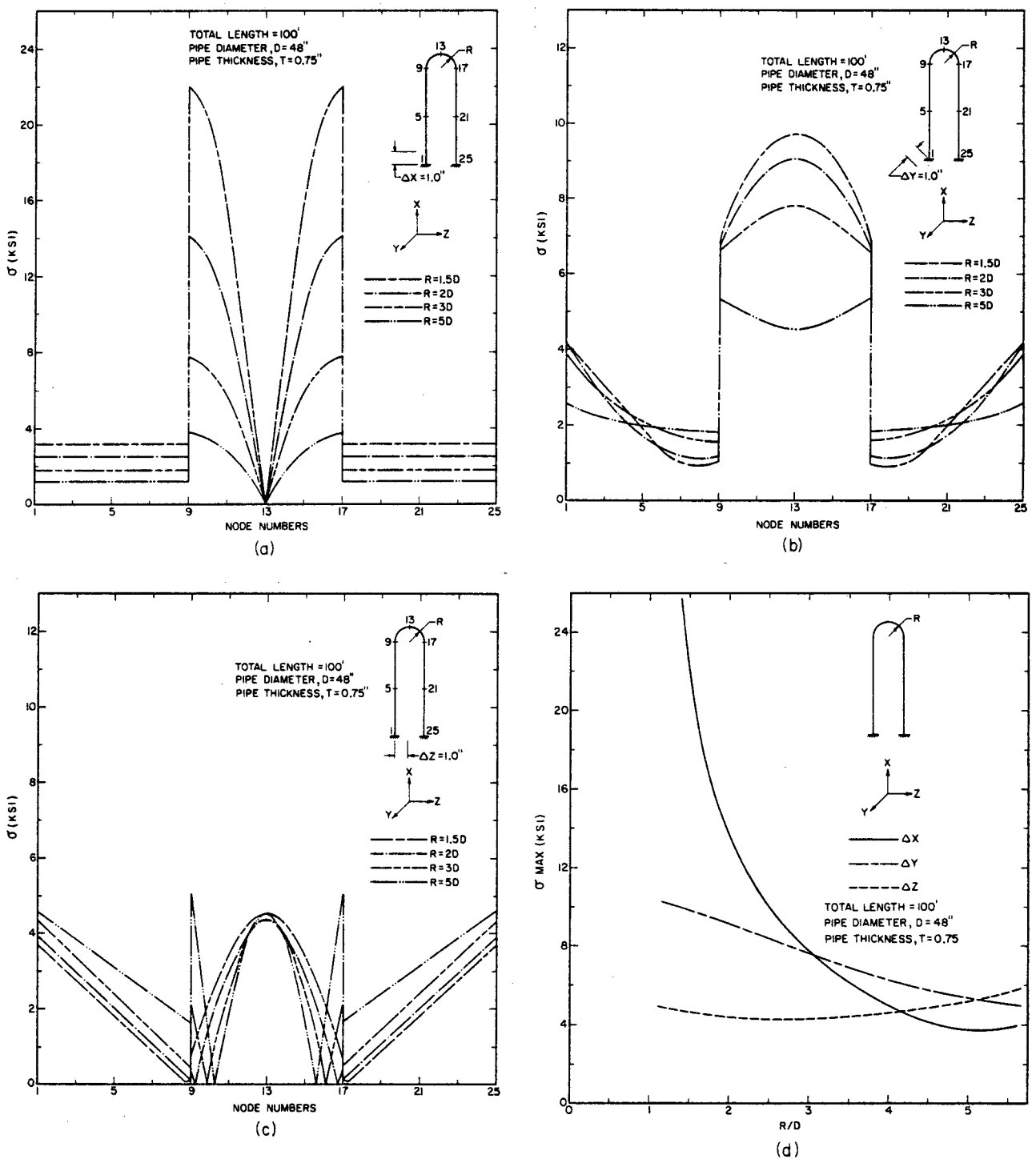

Figure III.1 Stress Distribution of a One-hump Hairpin Loop.
(a) displacement in the X-direction
(b) displacement in the Y-direction
(c) displacement in the Z-direction
(d) maximum stress vs. bend radius

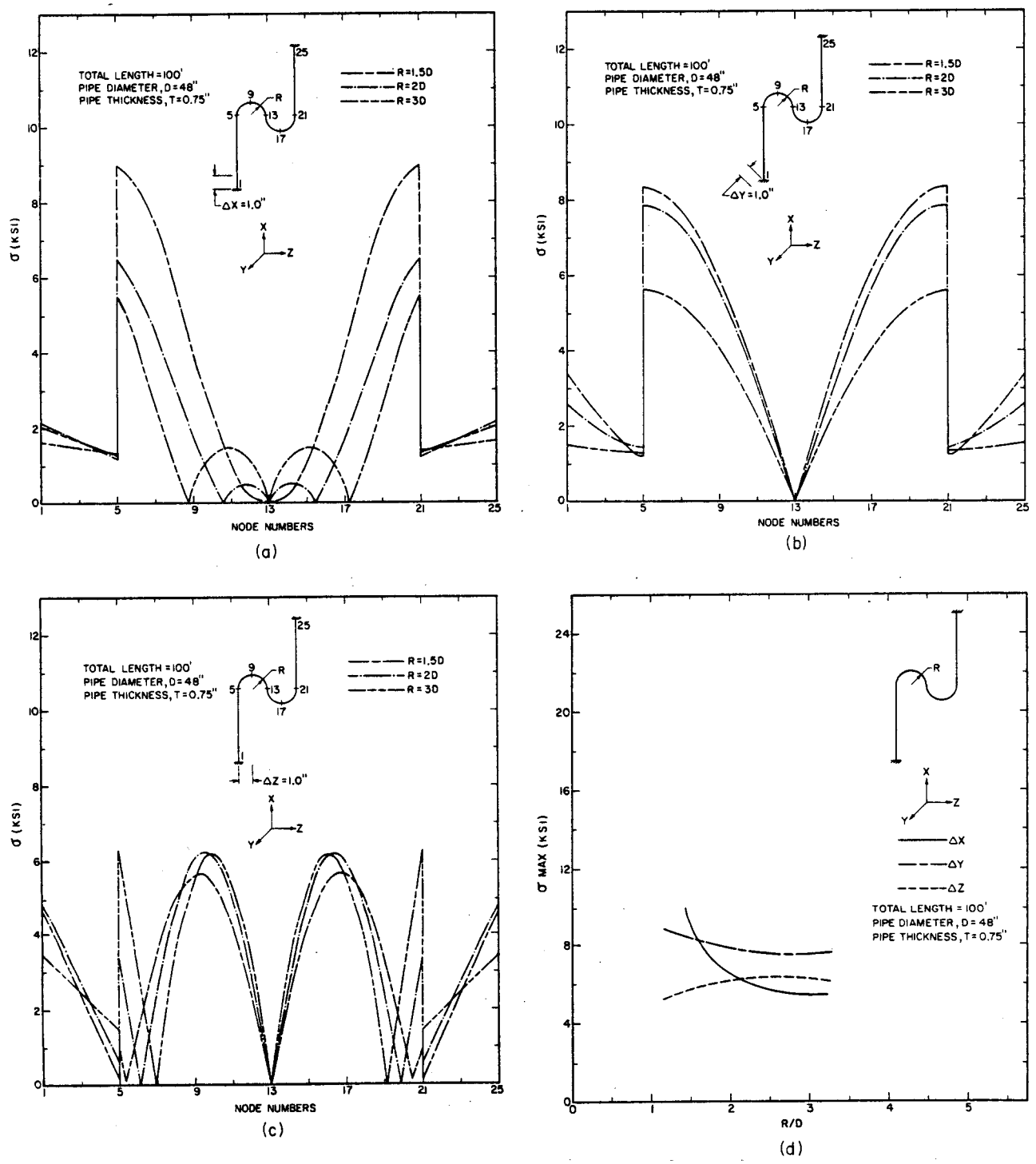

Figure III.2 Stress Distribution of a Two-hump Hairpin Loop.
(a) displacement in the X-direction
(b) displacement in the Y-direction
(c) displacement in the Z-direction
(d) maximum stress vs. bend radius

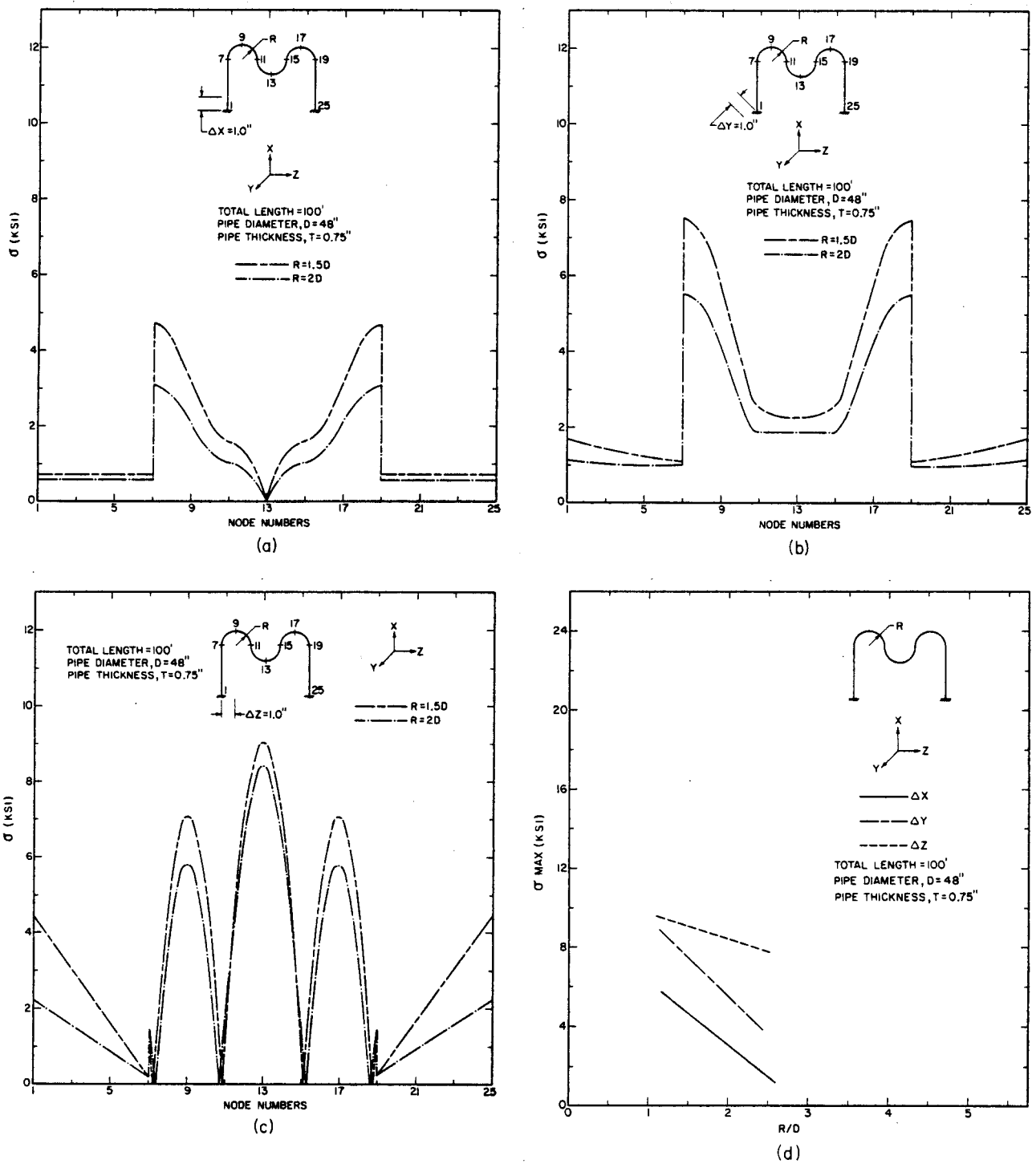

Figure III.3 Stress Distribution of a Three-hump Hairpin Loop.
(a) displacement in the X-direction
(b) displacement in the Y-direction
(c) displacement in the Z-direction
(d) maximum stress vs. bend radius

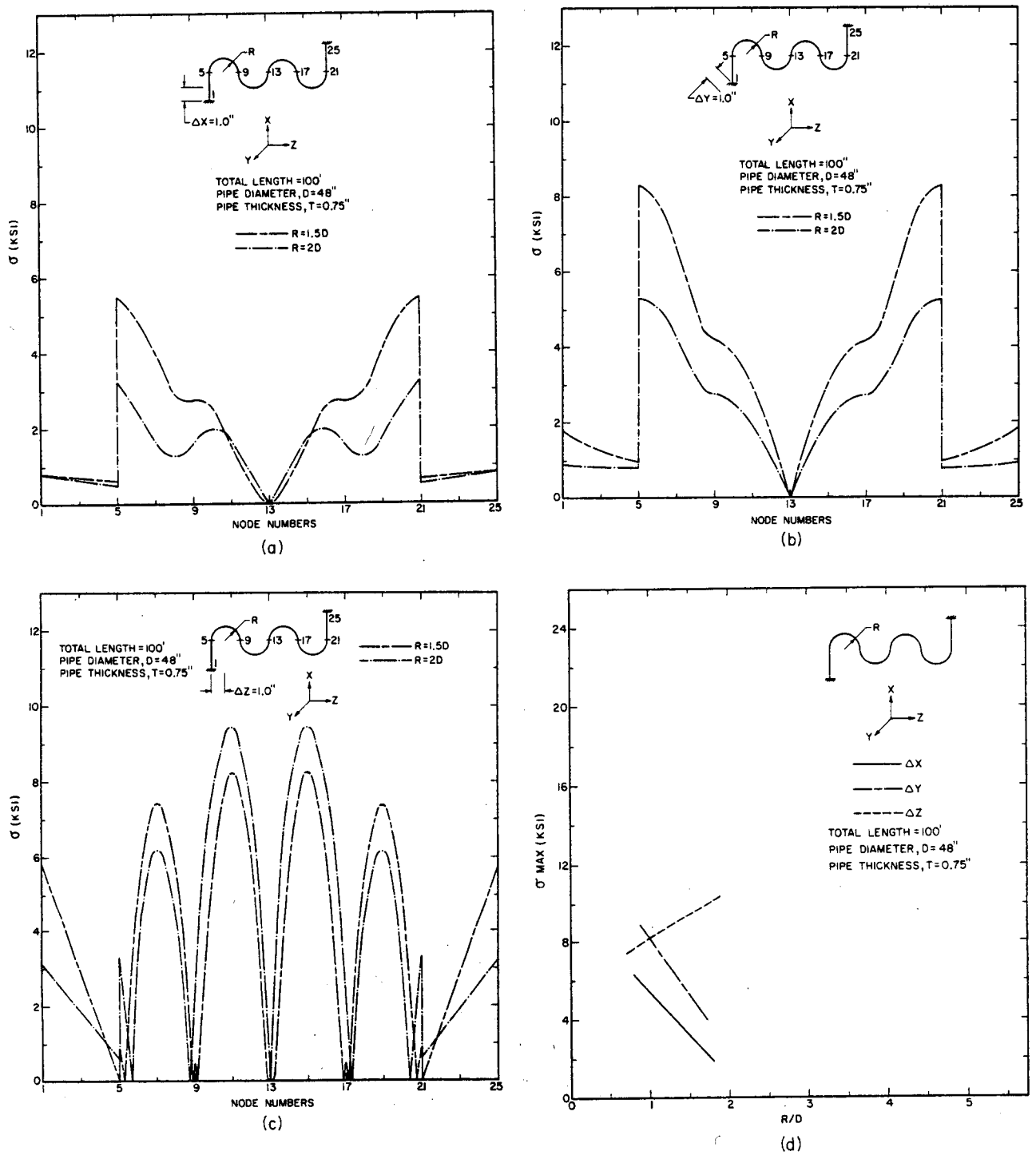

Figure III.4 Stress Distribution of a Four-hump Hairpin Loop.
(a) displacement in the X-direction
(b) displacement in the Y-direction
(c) displacement in the Z-direction
(d) maximum stress vs. bend radius

Figure III.5 shows the stress distribution of the coil loop. Nodes #5 and #21 at the cross over point of the loop are separated by a pipe diameter distance. Therefore, the configuration is not two dimensional as is the case for the other piping configurations. Figure III.5 (a) and (b) can be explained using the earlier reasoning. Although the displacement is in the Z-direction in Figure III.5 (c), the reactive moments are in all three directions due to the three dimensional configuration. Hence the stress distribution in the straight section is non-linear and the stress curves go through a minimum rather than zero because the resultant moment is not zero. In this case the maximum stress decreases when elbow radius increases. For the other two displacement components the stress go through a maximum as indicated in Figure III.5 (d). In these two cases when the elbow radius is small, the straight pipes are effective. When the elbow radius is small, the straight pipes are effective. When the elbow radius increases, the length of the straight pipe decreases and the stress increases. As the elbow radius increases further, the shorter straight pipe becomes ineffective and the effect of the elbow takes over, hence the stress decreases.

Figure III.6 and Figure III.7 can be explained in a similar manner. In these two configurations, the elbow changes radius at node #9 and node #17. Therefore, the stress curve shows additional discontinuity at these two points as compared to Figures III.1 through III.5. These two configurations also shows the general trend of decreasing stress with increasing elbow radius.

In summary some general observations made in this study are given as follows:

1. When the displacement is in the plane of the loop, the

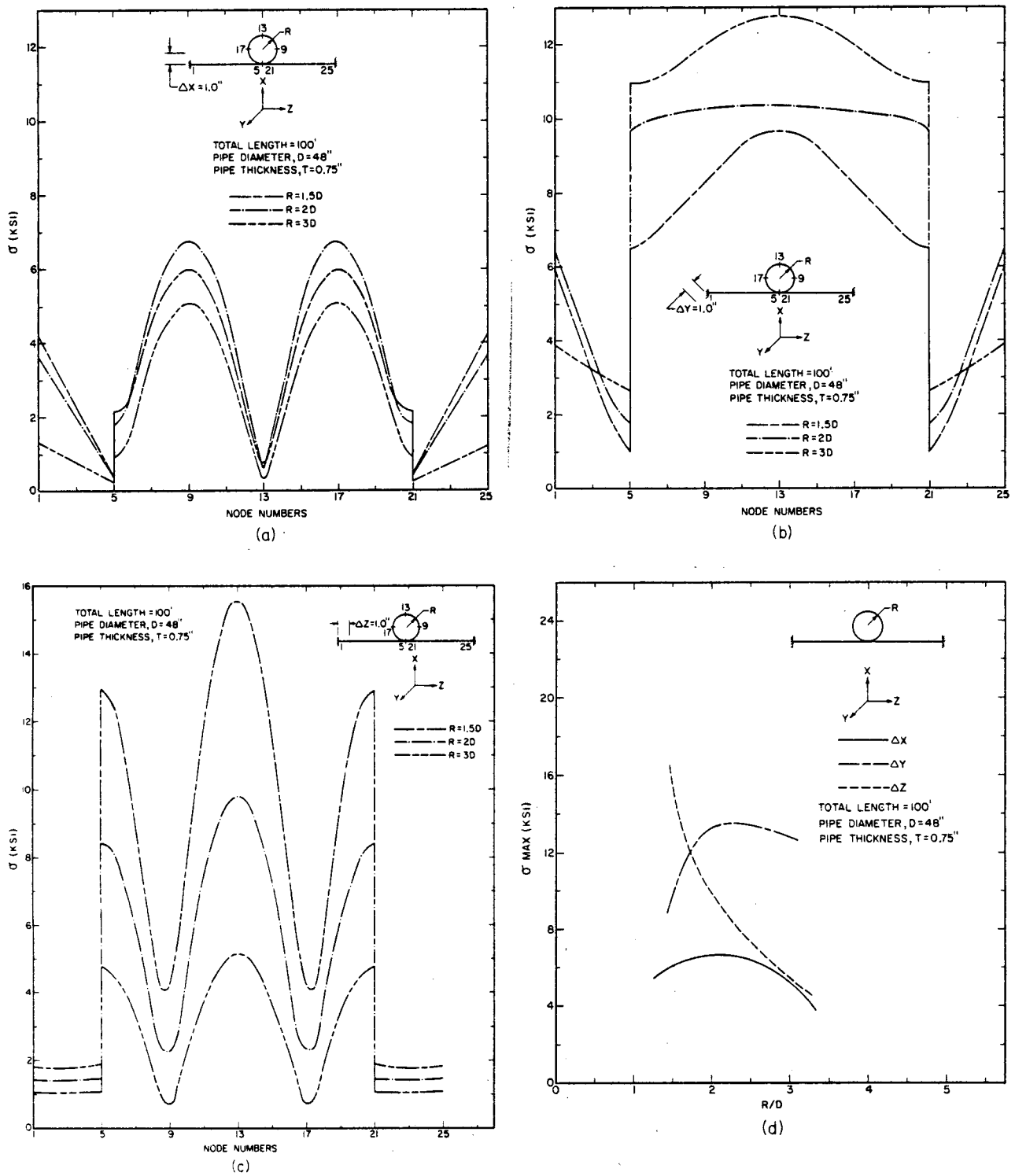

Figure III.5 Stress Distribution of a Coil Loop.
(a) displacement in the X-direction
(b) displacement in the Y-direction
(c) displacement in the Z-direction
(d) maximum stress vs. bend radius

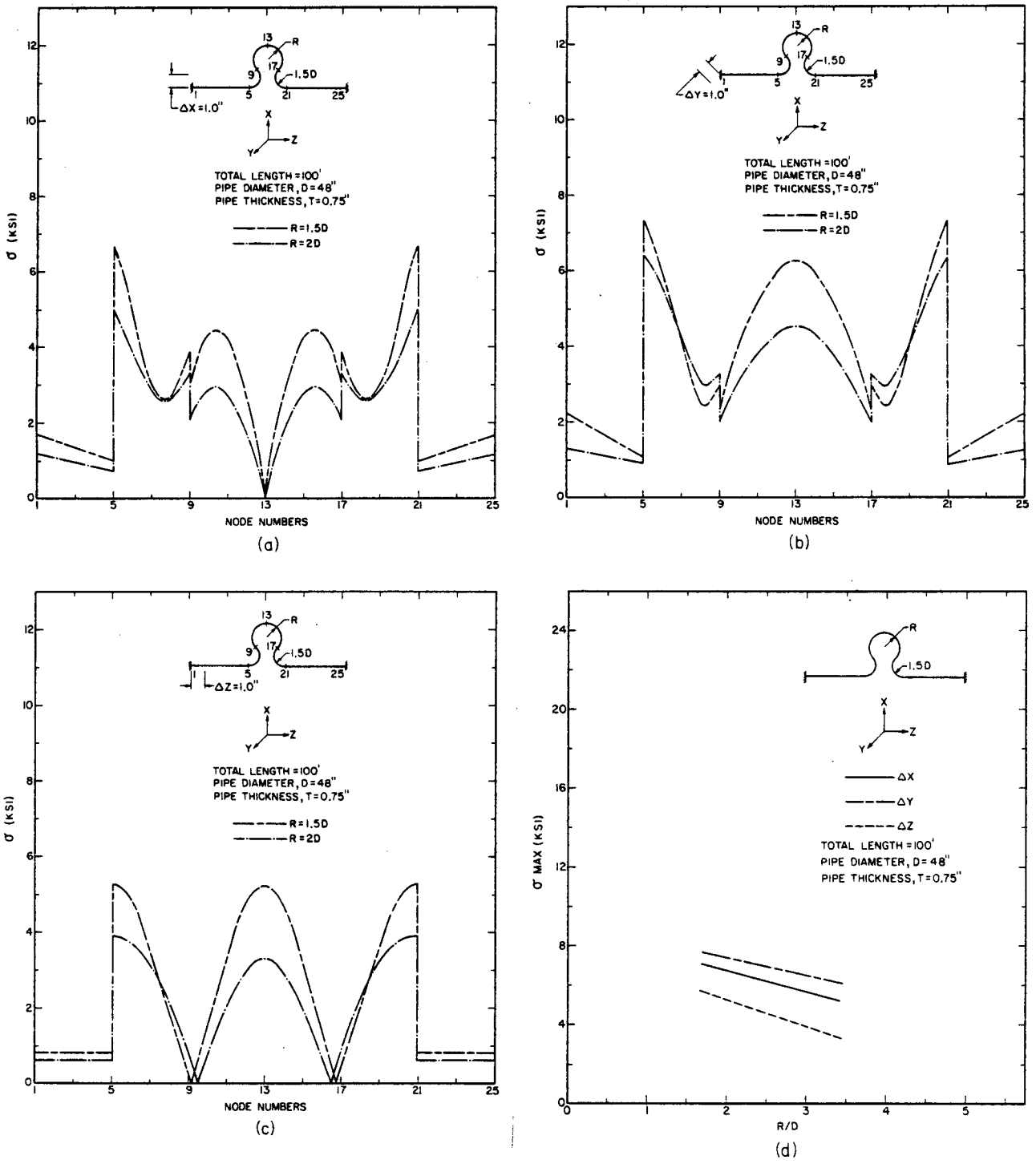

Figure III.6 Stress Distribution of an Omega Loop.
(a) displacement in the X-direction
(b) displacement in the Y-direction
(c) displacement in the Z-direction
(d) maximum stress vs. bend radius

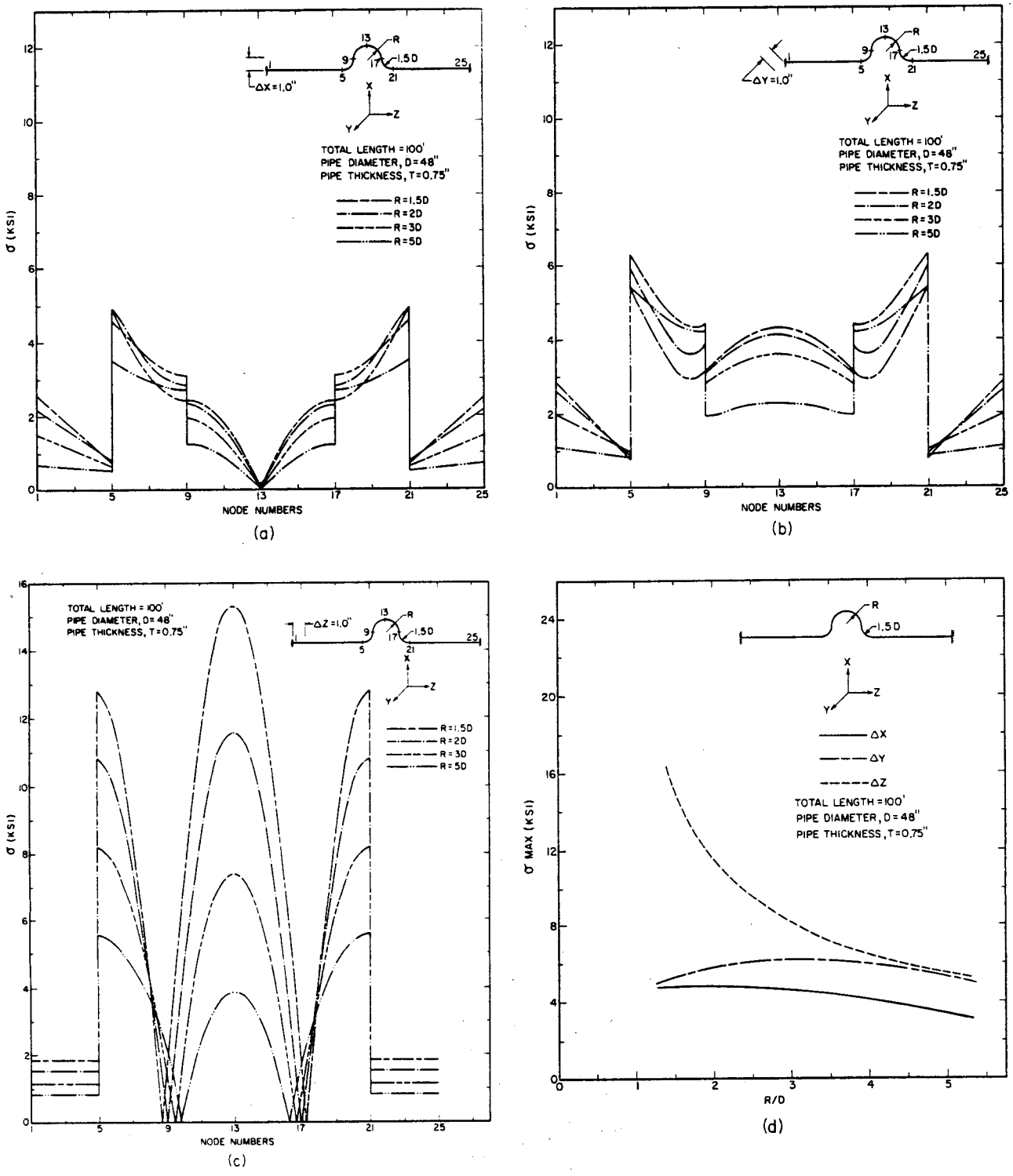

Figure III.7 Stress Distribution of a U-bend Loop.
(a) displacement in the X-direction
(b) displacement in the Y-direction
(c) displacement in the Z-direction
(d) maximum stress vs. bend radius

reactive forces is also in the same plane and the direction of the reactive moment is perpendicular to the plane. In this case the magnitude of the bending moment is linearly decreasing in the straight pipe. Hence, the stress curve is a straight line in the straight section.

2. When the displacement is out of the plane of the pipe, all three components of the force and moment are nonzero. Since the resultant moment is calculated as the root of the sum of the squares of each moment, the stress curve in the straight section is no longer a straight line.

3. The stress curve always has a discontinuity at the junction of a straight pipe and an elbow. This is due to the stress intensification factor of the elbow as indicated in Eq. (II.9) if $X = \ell$. If the end effect of the elbow is considered, the stress curve would be continuous and without a jump.

4. The bending moment in the elbow varies as a combination of trigonometric and quadratic functions as shown in Eq. (II.9) and (II.11).

5. For the same configuration, increasing the radius of the pipe bend increases the length of the elbow to accommodate thermal expansions. Therefore, the stress tends to decrease when the pipe bend radius increases. The same reasoning holds when the number of elbows is increased.

6. The straight section of the pipe serves to enhance the deflection of the elbow. Therefore, it is desirable to

have a long section of straight pipe perpendicular to the direction of anchor movement.

The maximum stress in different piping configurations are summarized in Figures (III.8) to (III.10). These curves can be explained by the general observations.

The second part of the study examines the same configurations except the span of the pipe instead of the total length is kept constant. The results of these analysis are shown in Figures (III.11) and (III.12). From these curves it is noted that the stress decreases monotonously as the radius of the elbow increases. This happens because, in a constant span study, the total length of the pipe increases with increasing elbow radius. Therefore, more elbow length is available to accommodate thermal expansion.

III.2 MARC Finite Element Program

The particular element which is of interest in a piping design is the elbow element #17 [7]. This element is a symmetrically loaded shell element specially modified for studying pipe bend. The theory and the results of the computation are given in Ref. [4] for an in-plane bending moment. A MARC analysis of elbows subjected to out-of-plane bending moment can be found in Ref. [5]. The curves obtained in Ref. [4] and [5] are recapitulated in Figures (III.13) to (III.17). These results are confirmed in this study using the MARC Program.

Figures (III.13) to (III.14) are for an elbow with a pipe factor h = 0.0924 and R/D = 1.475. In this case, an ASME code calculation gives:

$$B_2 = 0.75 \frac{1.95}{h^{2/3}} = 7.16$$

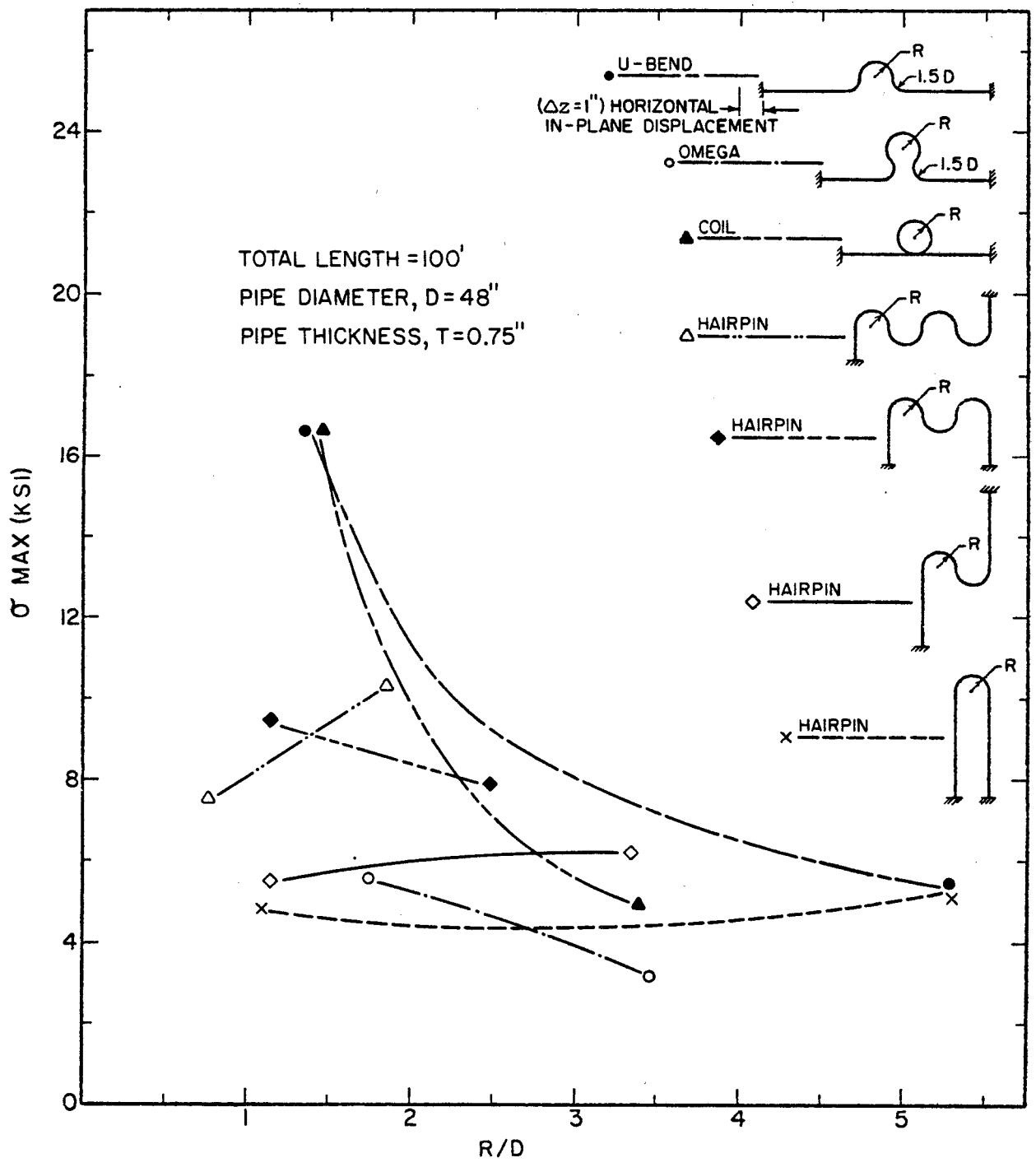

Figure III.8 Maximum stress in different piping configurations of constant lengths due to a constant anchor displacement in the z-direction.

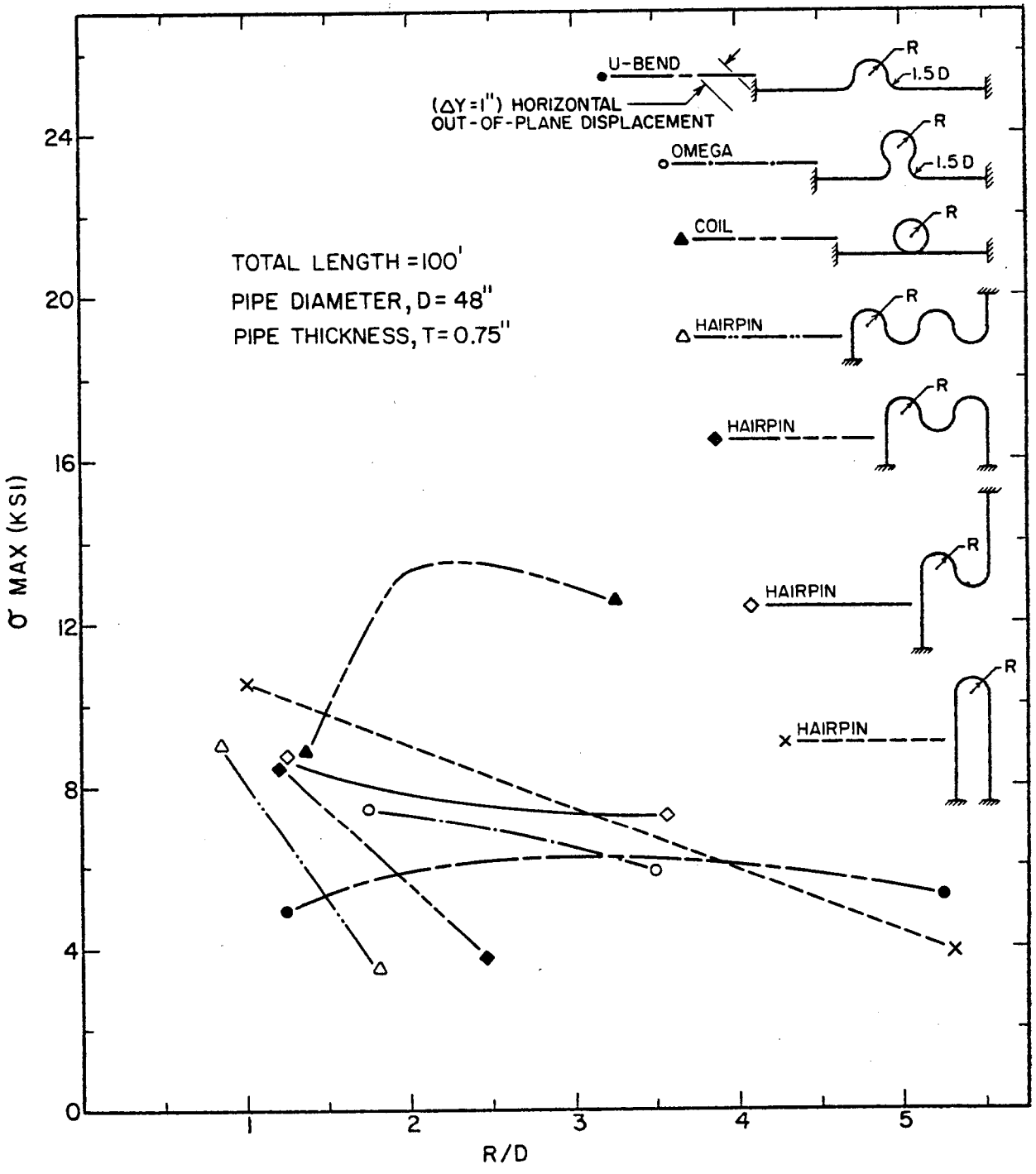

Figure III.9 Maximum stress in different piping configurations of constant lengths due to a constant anchor displacement in the Y-direction.

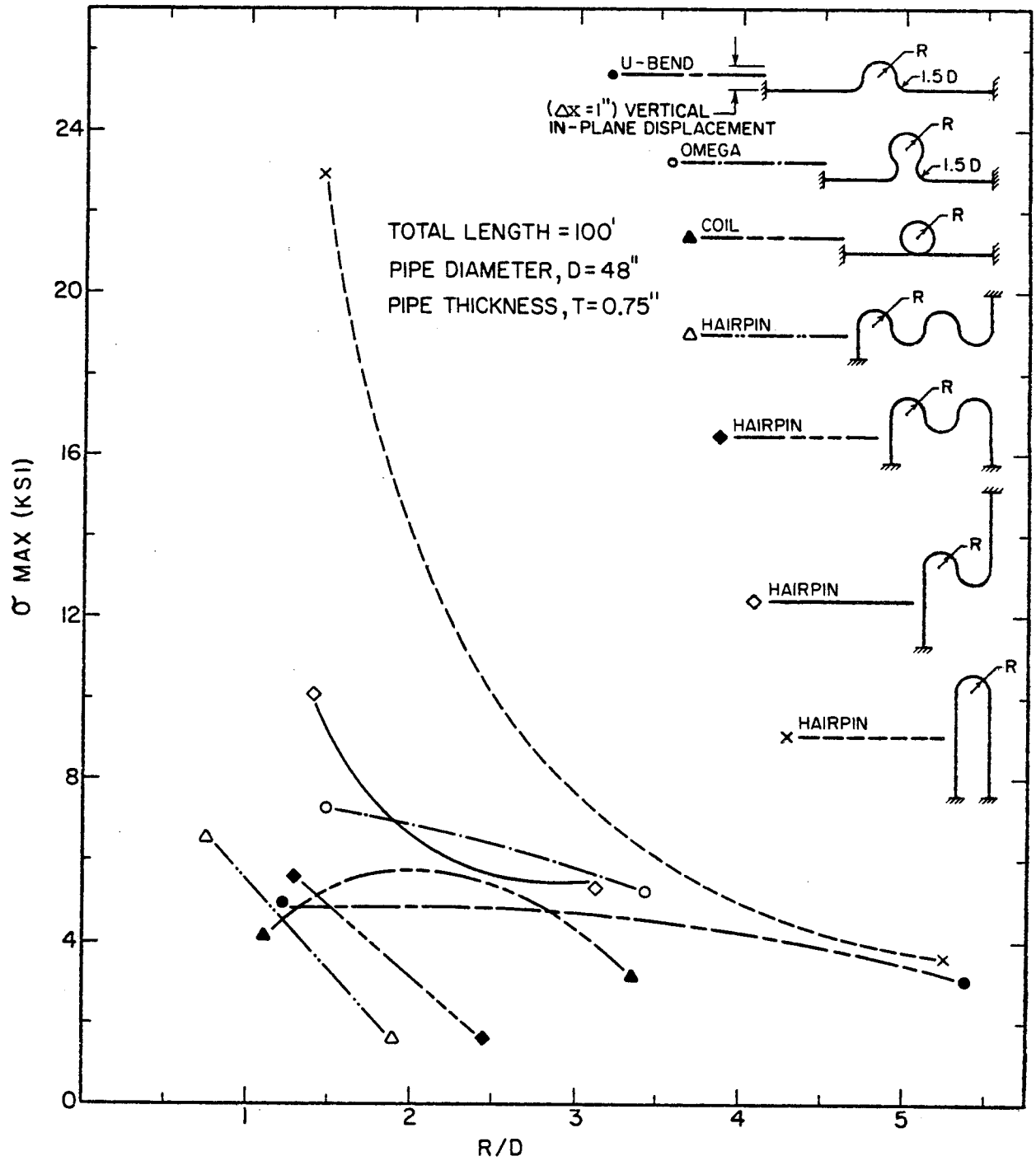

Figure III.10 Maximum stress in different piping configurations of constant lengths due to a constant anchor displacement in the X-direction.

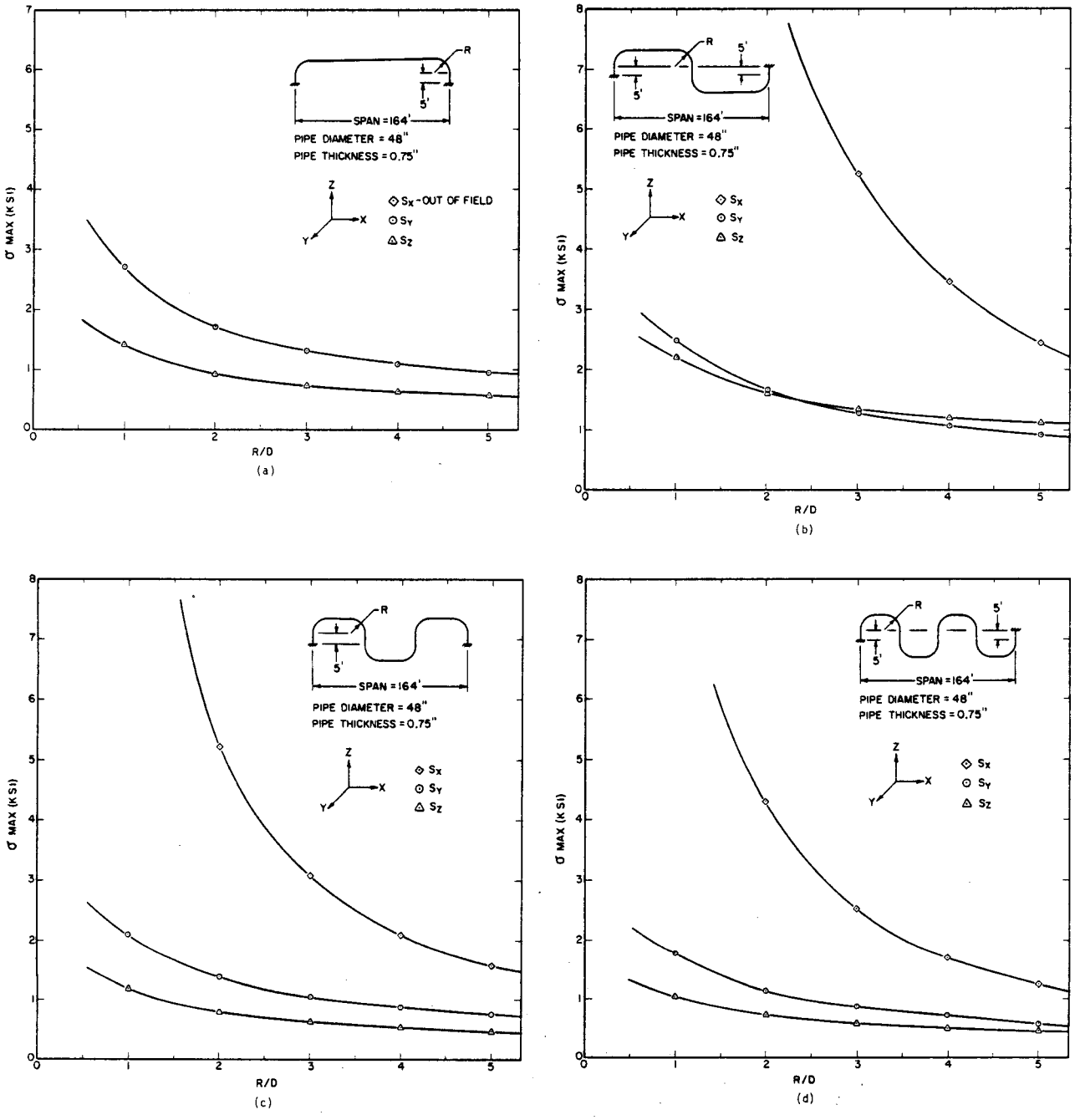

Figure III.11 Maximum Stresses of Hairpin Loops of Constant Span Due to a Constant 1" Anchor Displacement vs. Bend Radius.
(a) one hump hairpin (b) tow hump hairpin
(c) three hump hairpin (d) four hump hairpin

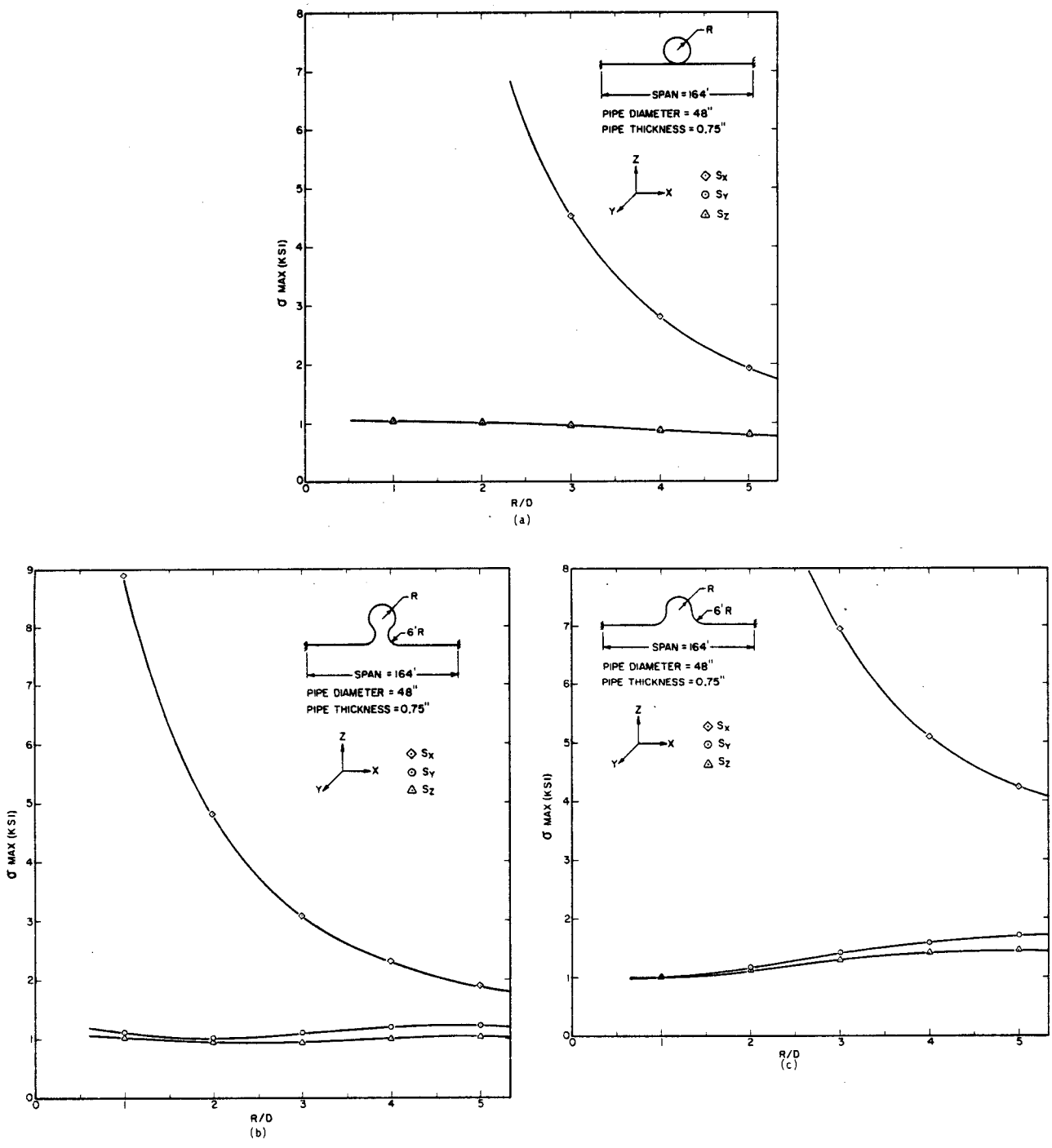

Figure III.12 Maximum stresses of different piping configurations of constant span due to a constant 1" anchor displacement vs. bend radius.
(a) coil loop
(b) omega loop
(c) U-bend loop

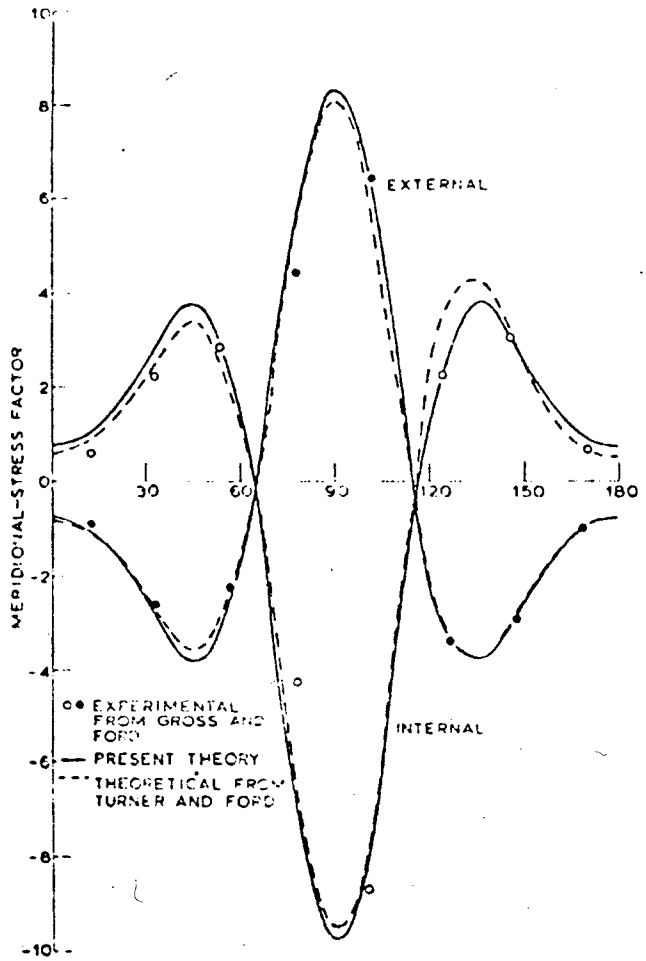

Figure III.13 Distribution of Meridional Stress for an Elbow Subjected to in-plane bending moment (from Ref. [4]).

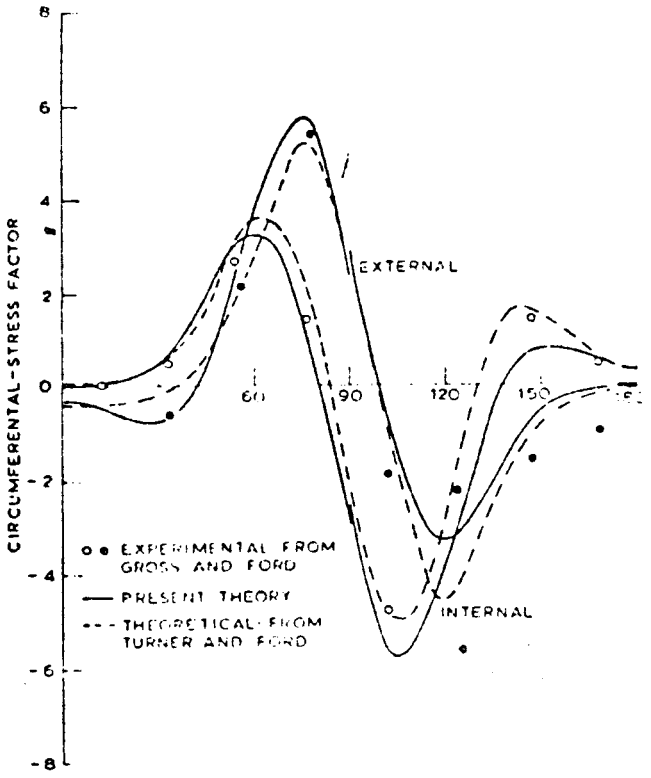

Figure III.14 Distribution of Circumferential Stress for an elbow subjected to in-plane bending moment (from Ref. [4]).

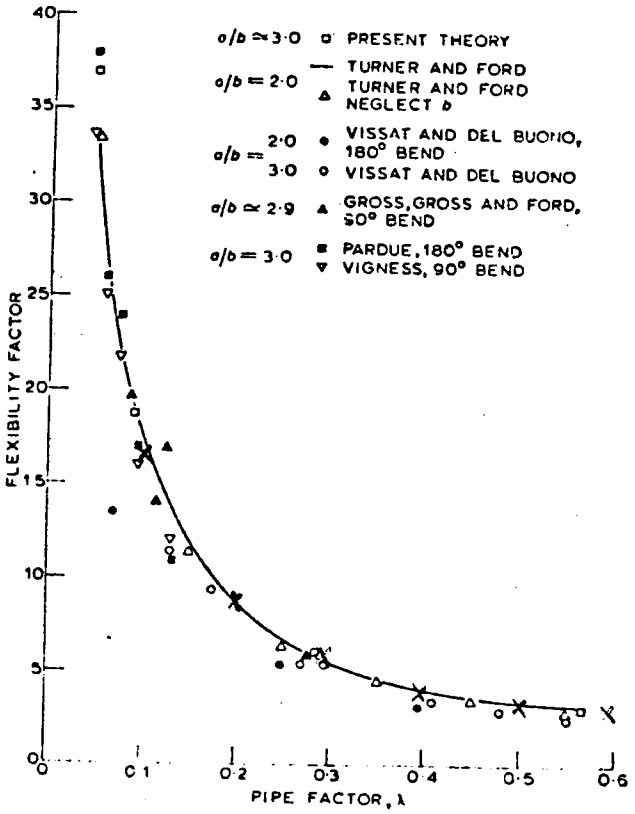

Figure III.15 Piping Flexibility Factors (from Ref. [4]). ASME Code Values are marked with crosses.

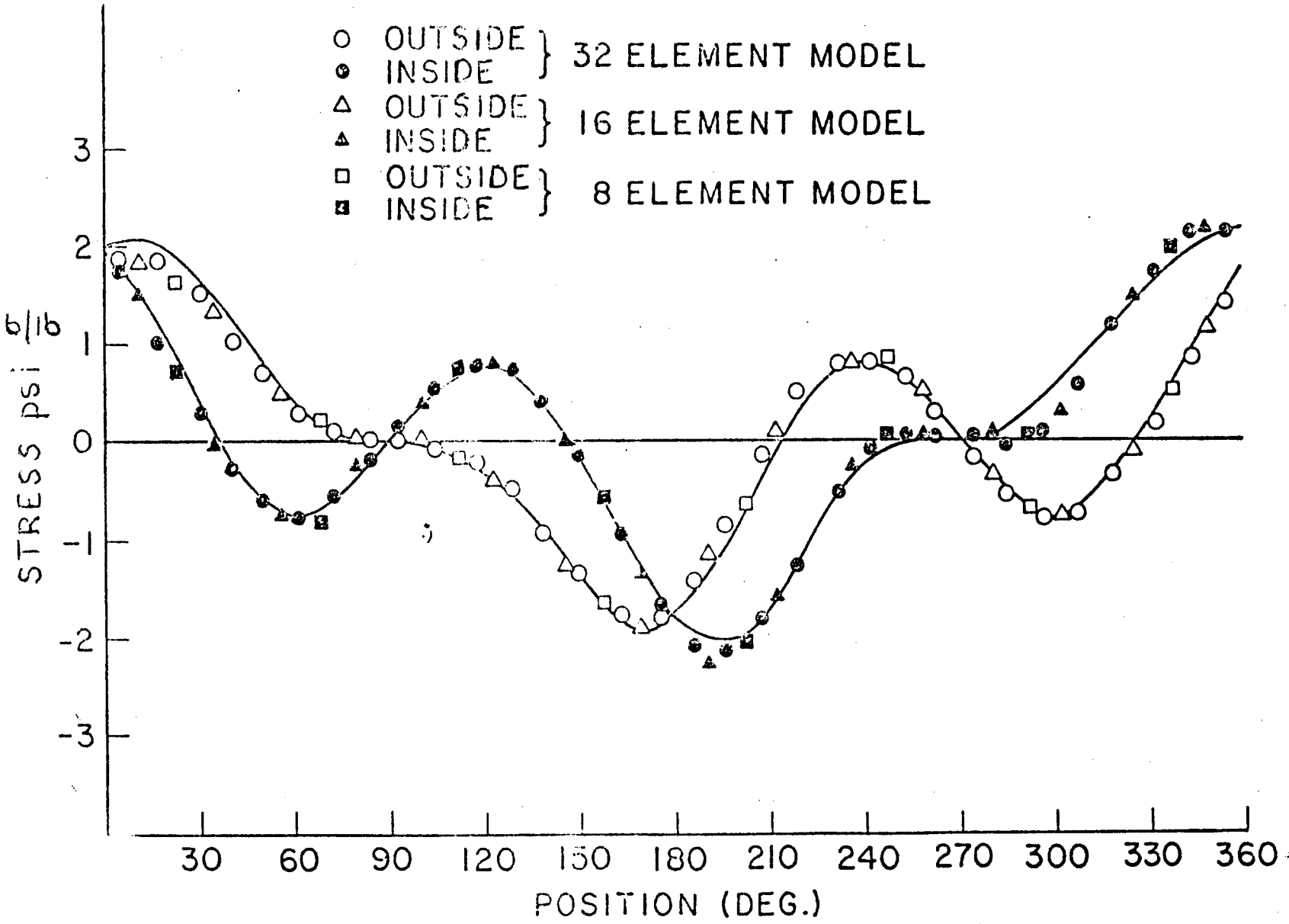

Figure III.16 Longitudinal Stress for an Elbow Subjected to out of plane Bending Moment (from Ref. [5]).

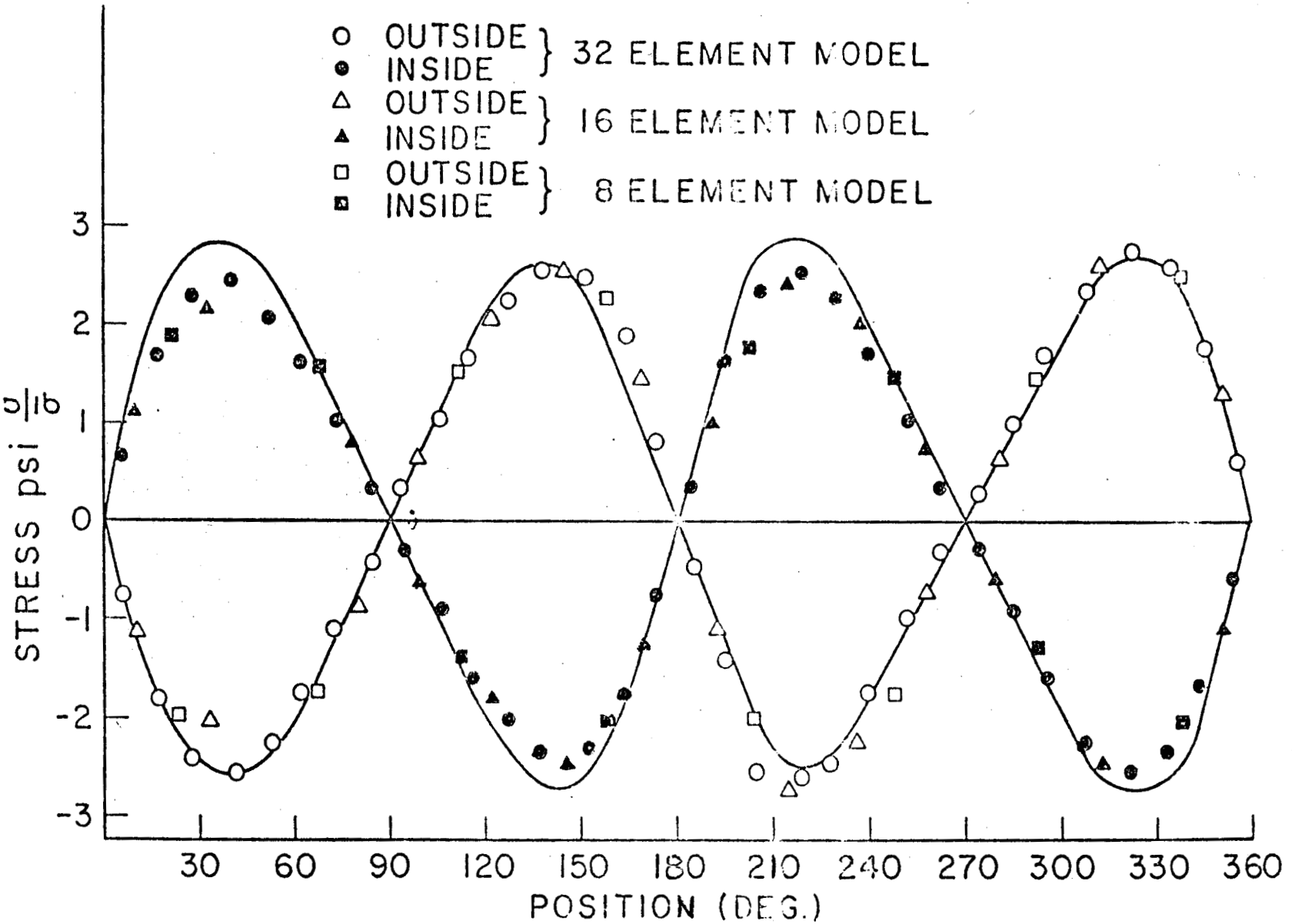

Figure III.17 Circumferential Stress for an Elbow Subjected to out of plane Bending Moment (from Ref. [5]).

$$C_2 = \frac{1.95}{h^{2/3}} = 9.55. \qquad \text{(III.1)}$$

The code calculation values of the flexibility factor are shown in Fig. (III.15) by cross mark symbols. In Figs. (III.16) and (III.17), the elbow dimensions are

$$t = 0.244$$

$$D = 6.312$$

$$R = 18.23.$$

Hence the stress intensification factors are

$$B_2 = 2.5$$

$$C_2 = 3.338 \qquad \text{(III.2)}$$

All the ASME code calculations compare fairly well with the curves.

A thermal stress check run is also made for a 90° elbow with a 36" O.D., 5" thickness and 54" bend radius subjected to 950° F on the inner surface and 750° F on the outer surface. The thermal stress agrees with the analytic result for a cylindrical shell [6].

$$\sigma = \frac{E\alpha\Delta T}{2(1 - \nu)}$$

$$= \frac{30 \times 10^6 \times 9.8 \times 10^{-6} \times 200}{2(1 - 0.3)}$$

$$= 42{,}000 \text{ psi} \qquad \text{(III.3)}$$

REFERENCES

1. ASME Pressure Vessel and Piping Code; Section III.

2. Timoshenko, S.P., "Strength of Materials", D. Van Nostrand Co., Inc., Third Ed., 1955.

3. "An Assessment of Basic Approaches to the Design of the Primary System of Loop Type LMFBR's", Primary System Study Group, July 1977.

4. Marcal, P.V., "Elastic-Plastic Behavior of Pipe Bends with In-Plane Bending", Journal of Strain Analysis, 2(1), 84, 1967.

5. Dodge, N.G. and Moore, S.E., "Stress Indices and Flexibility Factors for Moment Loadings on Elbows and Curved Pipes", ORNL-TM-3658, Oak Ridge National Laboratory, March 1972.

6. Timoshenko, S.P. and Woinowsky-Krieger, S., "Theory of Plates and Shells", 2nd Ed., McGraw-Hill, 1959.

7. "MARC-CDC User Information Manual", Vol. 1-3, Version H, Control Data Corporation, 1976.